**Supporting Information**

# Scaling relationships for the elastic moduli and viscosity of mixed lipid membranes

Elizabeth G. Kelley,[a] Paul D. Butler,[a,b,c] Rana Ashkar,[d,e] Robert Bradbury,[a,f] Michihiro Nagao[a,f,g]

[a] Center for Neutron Research, National Institute of Standards and Technology, Gaithersburg, MD, 20899
[b] Department of Chemical and Biomolecular Engineering, University of Delaware, Newark, DE, 19716
[c] Department of Chemistry, The University of Tennessee, Knoxville, TN, 37996
[d] Physics Department, Virginia Tech, Blacksburg, VA 20461
[e] Center for Soft Matter and Biological Physics, Virginia Tech, Blacksburg, VA 20461
[f] Center for Exploration of Energy and Matter, Indiana University, Bloomington, IN, 47405
[g] Department of Physics and Astronomy, University of Delaware, Newark, DE 19716

## S1. Lipid mixtures



## S2. Lipid volume



## S3. Bilayer structure



## S4. Bilayer dynamics

# S1. Lipid mixtures

**Table S1.** Composition of protiated lipid samples. $x_{DSPC}$ refers to the mole fraction of DSPC in the protiated lipid mixtures.

| $x_{DSPC}$ | mass fraction | |
|---|---|---|
| | **DMPC** | **DSPC** |
| 0 | 1 | 0 |
| 0.3 | 0.67 | 0.33 |
| 0.5 | 0.46 | 0.54 |
| 0.6 | 0.36 | 0.64 |
| 0.7 | 0.27 | 0.73 |
| 1 | 0 | 1 |

**Table S2.** Composition of tail-deuterated lipid samples. $x_{DSPC\text{-}d70}$ refers to the total mole fraction of DSPC in the tail-deuterated lipid mixtures.

| $x_{DSPC\text{-}d70}$ | mass fraction | | | |
|---|---|---|---|---|
| | **DMPC** | **DMPC-$d_{54}$** | **DSPC** | **DSPC-$d_{70}$** |
| 0 | 0.098 | 0.902 | - | - |
| 0.3 | 0.065 | 0.600 | 0.035 | 0.300 |
| 0.5 | 0.045 | 0.415 | 0.056 | 0.484 |
| 0.6 | 0.050 | 0.420 | 0.060 | 0.480 |
| 0.7 | 0.026 | 0.241 | 0.080 | 0.660 |
| 1 | - | - | 0.104 | 0.896 |

# S2. Lipid volume

**Densitometry data analysis**

The partial specific volume ($v_s$) was determined from measurements of the lipid solution density according to

$$v_s = \frac{1}{\rho_0}\left(1 - \frac{\rho_s - \rho_0}{c}\right) \qquad (S1)$$

in which $\rho_0$ is the solvent density, $\rho_S$ is the solution density, and c is the lipid concentration.(1, 2) The volume per lipid molecule ($V_L$) was then calculated according to

$$V_L = \frac{v_s}{N_A}\sum_i x_i M_i \qquad (S2)$$

in which $N_A$ is Avogadro's number and $x_i$ and $M_i$ are the component lipid mole fractions and molecular weights, respectively. The measured fluid phase volume per lipid were compared to values calculated according to

$$V_L'(T) = \sum_i x_i V_i(T) \qquad (S3)$$

in which $V_i$(T) are the molecular lipid volumes calculated according to work by Koenig and Gawrisch.(3) Data for the lipid mixtures are presented in Supplementary Table S3. The critical temperatures for the different samples, corresponding to the melting temperature in the pure lipid membrane and the onset of gel-fluid coexistence in the mixed lipid bilayers, were determined from the derivative of the measured volume vs. temperature curve and are listed in Table S3.(4, 5)

**Table S3**. Measured ($V_L$) and calculated ($V_L'$) lipid volumes at $T$ = 60°C. $T_m$ for the mixtures were determined from density measurements or DSC experiments. Experimental values for the lipid volume were determined from density measurements according to Eq. S2 and the calculated values were determined according to Koenig and Gawrisch, Eq. S3.(3) The calculated values are within 1 % of the measured values.

| $x_{DSPC\text{-}d70}$ | $T_m$ (°C) | $T$ = 60 °C | |
|---|---|---|---|
| | | $V_L$ (nm$^3$) | $V_L'$ (nm$^3$) |
| 0 | 20.5 | 1.123 | 1.123 |
| 0.3 | 36 | 1.205 | 1.192 |
| 0.5 | 45 | 1.233 | 1.238 |
| 0.6 | 46 | 1.269 | 1.261 |
| 0.7 | 48 | 1.286 | 1.284 |
| 1 | 50.5 | 1.353 | 1.353 |

# S3. Bilayer structure

## S3.1 SANS and SAXS data analysis

The bilayer thickness and area per lipid ($A_L$) were determined from small angle neutron (SANS) and X-ray (SAXS) scattering measurements; however, it is important to note that the different techniques are sensitive to different bilayer thicknesses. The high contrast between the protiated lipid headgroups and deuterated water measured with SANS defines the overall bilayer thickness ($d_B$), also known as the Luzzati thickness.(6-8) The thickness measured in SAXS is defined between the peaks in the electron density profile and corresponds to the distance between the lipid headgroup phosphates ($d_{pp}$). (6, 7) $d_B$ is on average $\approx 0.16$ nm larger than $d_{pp}$.(6)

Extracting the bilayer thickness requires an appropriate model of the scattering length density profile, which is determined by the volume probability profiles of the different components and their respective scattering contrasts. We use simplified form factor models from literature to fit the data at a single contrast.(9-11) We also compare $D_B$ values determined from SANS measurements at two different contrasts; protiated lipids in $D_2O$ and tail-deuterated lipids in $D_2O$ analyzed with different models to ensure that our assumptions in data analysis were not affecting the results. Importantly, the bilayer thicknesses from both data series are in excellent agreement (Figure S1).

SANS data for the protiated lipid vesicles were fit with a vesicle form factor in the SasView Program.(12) The model describes the bilayer as a single slab with a thickness that was assumed to represent $d_B$. The scattering length density (SLD) of the lipid bilayer was calculated from tabulated scattering factors and the measured lipid volumes. The only fit parameter in the analysis was the bilayer thickness.

SANS data for the tail-deuterated lipid bilayer were analyzed using a form factor model described in literature that uses a symmetric six-slab volume probability distribution with separate components for the lipid headgroups, $CH_2$ groups of the hydrocarbon chains, and terminal $CH_3$ groups at the bilayer midplane.(10, 11) The volume probability profile was convoluted with a Gaussian with a width of 2.8 Å to account for the effects of thermal disorder. (10, 11) The lipid volumes ($V_L$) were constrained to the measured values (Table S3, other data not shown), and the volume of the headgroup (0.331 $nm^3$) and terminal methyl groups (0.053 $nm^3$) were constrained to reported values to minimize the number of fitting parameters. (11) We note that recent results show that $V_L$ and the volume of the terminal methyl group change with temperature; however, our results were not sensitive to changes within the reported range.(13) The only fit parameter was the area per lipid ($A_L$), which was used to calculate the Luzzati bilayer thickness, $d_B = 2V_L/A_L$.

SAXS data were analyzed with a form factor for lipid bilayers that described the lipid bilayer scattering length density as the sum of three Gaussians, representing each headgroup and the hydrophobic tail region.(14) The scattering length densities of the dry lipid headgroups and lipid tails were calculated from the respective lipid volumes listed in Supplementary Table S3. The number of waters associated with each headgroup were fit and ranged from approximately 6 to 10 waters per headgroup in good agreement with results in literature.(7, 15, 16)

Data fits were restricted to a $q > 0.05$ $Å^{-1}$ for the SANS data and $q > 0.03$ $Å^{-1}$ for the SAXS data , at which the contributions from the vesicle form factor and any intervesicle interactions were negligible and the scattered intensity was solely from the lipid bilayer.(8, 17)

As seen in Figure S1, the data were well fit by the simplified form factor models. While we are not able to extract the detailed volume probability profiles of the individual components as

in other methods, the values determined for $d_B$ (and correspondingly, $A_L$) are in good agreement with values reported from more detailed analysis methods (Figure S1 d).(8, 18)

For calculations at temperatures for which SANS data were not collected, the bilayer thickness was estimated from the measured bilayer expansivity, $\alpha_d = (1/d_B)(\partial d_B/\partial T)$ (Supplementary Table S4), and the presented error represents the propagated uncertainty in the calculated value.

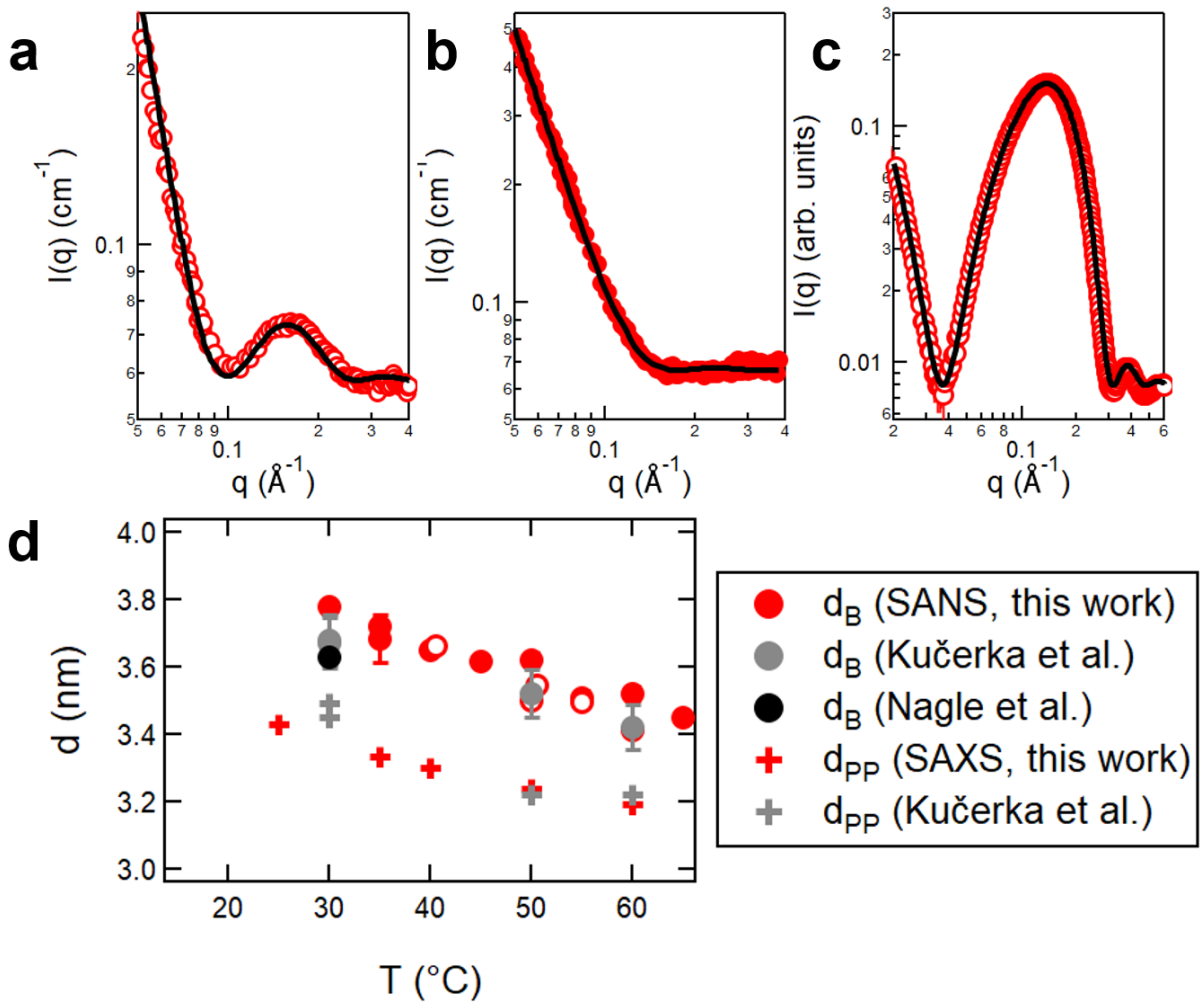


**Figure S1.** Representative SANS data for (**a**) tail-deuterated and (**b**) tail-protiated DMPC bilayers, as well as (**c**) SAXS for tail-deuterated DMPC bilayers, all measured at 50 °C. Solid lines are the form factor fits described in the supplementary text. (**d**) Summary of Luzzati thicknesses ($d_B$) from SANS and phosphate-to-phosphate thicknesses ($d_{PP}$) from SAXS as a function of temperature for the samples measured in the present work compared to the values reported by Kučerka et al.(8) and Nagle et al.(18) Open symbols correspond to $d_B$ values measured for tail-deuterated bilayers and closed symbols correspond to tail-protiated bilayers.

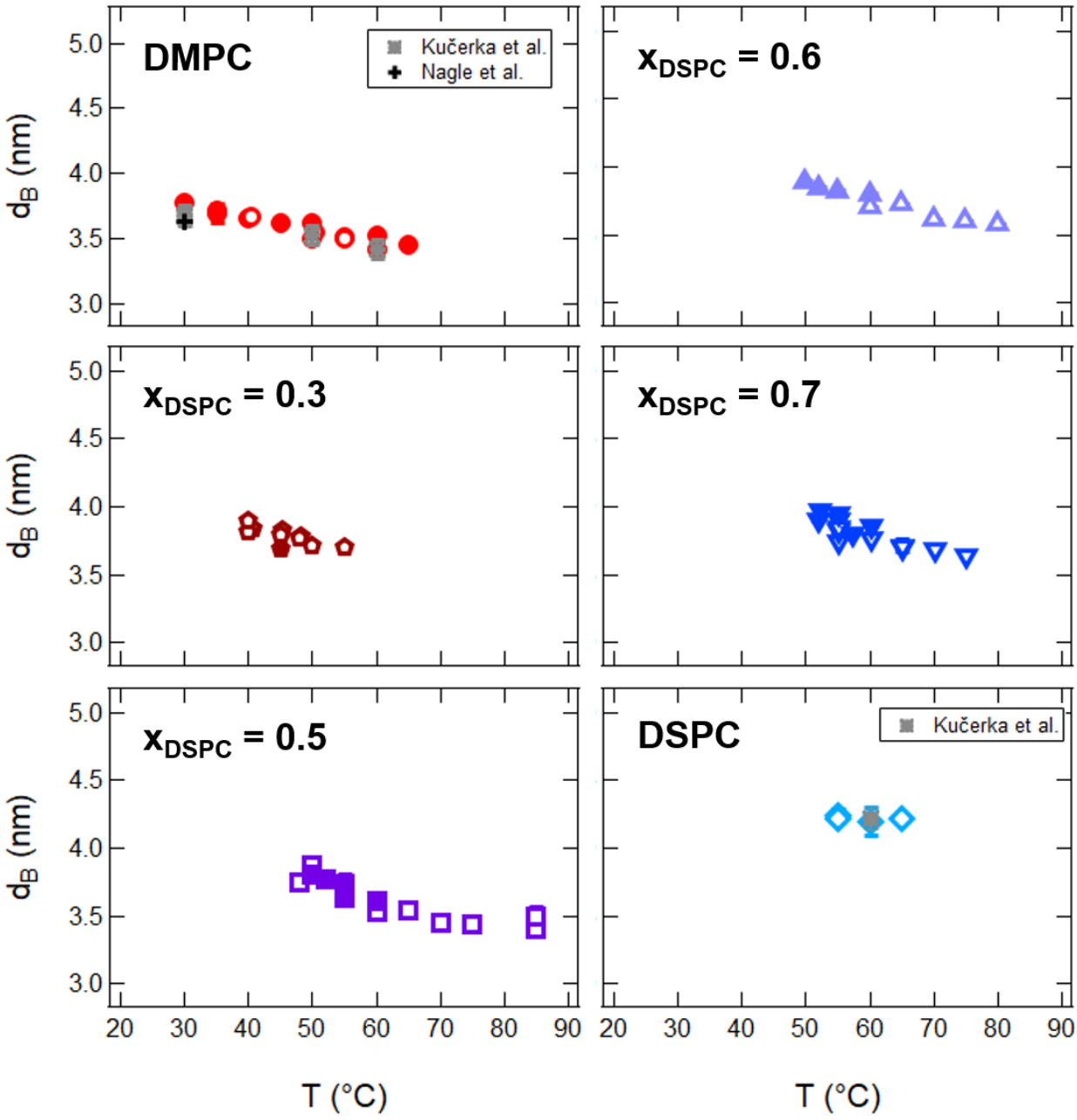


**Figure S2.** Measured bilayer thickness versus temperatures for the pure component and mixed lipid bilayers in the fluid phase. The bilayer composition is given by the text label on the plot. Open and closed symbols correspond to bilayers composed of tail-deuterated and protiated lipids, respectively. The stars and crosses on the plots for DMPC and DSPC are values taken from literature from Kučerka et al.(8) and Nagle et al.(18) as indicated in the legend. Bilayer thicknesses were determined from SANS data analysis as described in the supplementary text.

### S3.3 Fluid phase expansivities

The thermal expansion coefficients were determined from a linear fit to the measured bilayer thickness versus temperature. The temperature dependence of the thickness changes for the pure components and mixtures ranged from (-0.04 to -0.07) Å/°C which is consistent with the average value reported for saturated phospholipids of -0.059 Å/°C.(8, 19) Reported in Table S4 are the calculated thermal expansivities $\alpha_{d_B} = (1/d_B)(\partial d_B/\partial T)$ from the neutron scattering fit results.

**Table S4**. Calculated thermal expansivities, $\alpha_{d_B} = (1/d_B)(\partial d_B/\partial T)$, at T = 60 °C obtained from the neutron scattering fitting results. The presented uncertainty is the propagated uncertainty from the fit results.

| $x_{DSPC\text{-}d70}$ | T = 60 °C | |
|---|---|---|
| | $d_B$ (nm) | α (°C$^{-1}$) |
| 0 | 3.45 ± 0.06 | -0.0024 ± 0.0001 |
| 0.3 | 3.65 ± 0.01 | -0.0023 ± 0.0001 |
| 0.5 | 3.57 ± 0.06 | -0.0028 ± 0.0006 |
| 0.6 | 3.75 ± 0.05 | -0.0026 ±0.0001 |
| 0.7 | 3.82 ± 0.06 | -0.0022 ±0.0001 |
| 1 | 4.21 ± 0.02 | -0.0037 ±0.0009 |

# S4. Bilayer dynamics

### NSE data analysis

NSE is a quasielastic scattering technique that probes dynamics on nanometer length scales and nanosecond time scales, making it a well-suited technique to study bilayer fluctuation dynamics. NSE data are reported as the intermediate scattering function (ISF), *I(q,t)/I(q,0),* which represents the probability of finding atomic correlations at a given distance (measured as $q$ in reciprocal space, which corresponds to $2\pi/q$ in real space) after a given amount of time (Fourier time, $t$). Thus, the value of the intermediate scattering function decays with increasing Fourier time as the bilayer fluctuates and the correlations decrease. The data are described by a decay rate, Γ, which, for single membrane bending fluctuations, are well described by a stretched-exponential as developed by Zilman and Granek(20)

$$\frac{I(q,t)}{I(q,0)} = exp\left[-(\Gamma(q)t)^{2/3}\right] \qquad (S4)$$

The decay rate is $q$ dependent and, for single membrane bending fluctuations, as shown by Zilman and Granek (20), follows a $q^3$ dependence with a slope that is inversely proportional to the membrane stiffness with effective bending modulus, $\tilde{\kappa}$. Watson and Brown suggested that $\tilde{\kappa} = \kappa + d^2K_{A,m}$ where the first term accounts for the contribution of the membrane elastic properties to the measured membrane undulations and the second term accounts for the contribution from the dissipation within the membrane itself. (21) $\kappa$ is the intrinsic bending modulus measured with techniques such as diffuse X-ray scattering or micropipette aspiration, $d$ is the height of the neutral surface, and $K_{A,m}$ is the monolayer compressibility modulus. Using published relationships between $K_{A,m}$ and $\kappa$, and assuming that the neutral surface lies at the interface of the hydrophilic headgroups and the hydrophobic tails gives the following expression for Γ

$$\Gamma = 0.0069 \frac{k_B T}{\eta_{D_2O}} \sqrt{\frac{k_B T}{\kappa}} q^3 \qquad (S5)$$

in which $k_B$ is the Boltzmann constant, $T$ is the temperature, $\eta_{D_2O}$ is the viscosity of the $D_2O$ surrounding medium. (22) All variables in this expression for the measured NSE decay constant are known quantities with exception of κ, allowing direct determination of the bending modulus from the slope of the $\Gamma$ versus $q^3$ plot (Figure S3b). We note that here we have adopted the widely-used Zilman-Granek formalism to extract κ from the NSE measurements as well as made assumptions about the values of $K_{A,m}$ and d. While there may be other approaches to determining κ from NSE data, we emphasize the extracted Γ values from the NSE data are inversely related to the membrane stiffness regardless of the assumptions as exemplified in Figure S7. Changing the relationship between $\tilde{\kappa}$ and $\kappa$ or values of $d$ and/or $K_{A,m}$ would systematically shift all of the values of κ but would not change the main result that the dynamics and associated membrane properties scale with $A_L$.

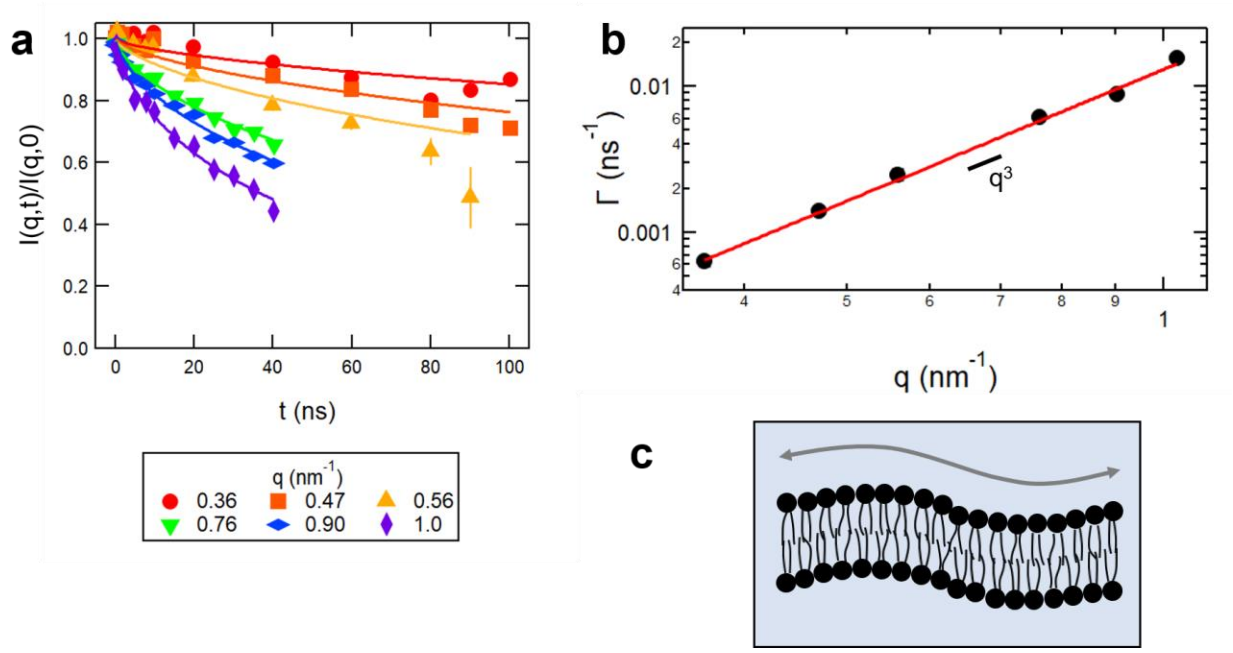


**Figure S3**. Neutron spin echo data (NSE) for bending fluctuations measurements of $x_{DSPC}$ = 0.6 at  at $T$ = 70 °C ($T$ - $T_m$ = 21 °C). (**a**) Measured intermediate scattering function (points) and fits to a stretched exponential according to Eq. S4 (lines) (**b**) Corresponding relaxation rates ($\Gamma$) extracted from the fits to the ISF (points) and the fit (solid line) to the modified Zilman-Granek model given in Eq. S5 showing a $q^3$ scaling. (**c**) Schematic illustration of the scattering length density contrast between protiated lipids in $D_2O$ used to measure collective membrane bending fluctuations.

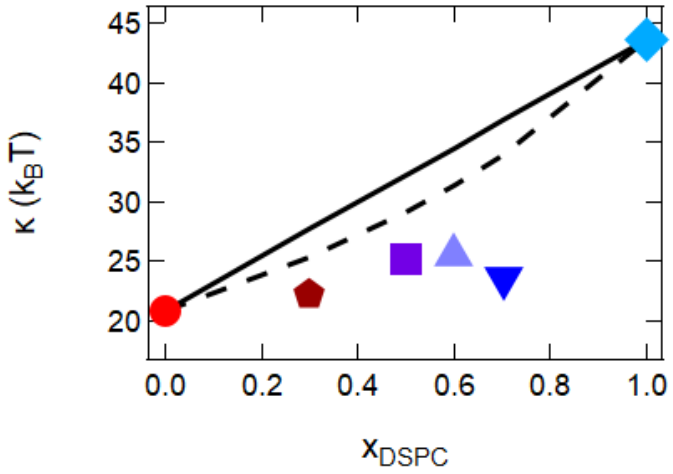


**Figure S4**. Bending modulus versus composition determined from NSE measurements at T = 65 °C. The points are measure data and the solid and dashed lines correspond to the linear and arithmetic average of the pure component properties, respectively.

Recent experimental works have also measured collective thickness fluctuations out of the plane of the membrane using NSE.(23-26) The thickness fluctuations were seen as excess dynamics at length scales corresponding to the bilayer thickness, characterized by a deviation from the $\Gamma \propto q^3$ behavior predicted from single membrane bending fluctuations (Figure S5b). The excess dynamics were characterized using two additive decay constants

$$\Gamma = \Gamma_{bend} + \Gamma_{thickness} \qquad (S6)$$

which are given by the empirical expression

$$\Gamma = 0.0069 \frac{k_B T}{\eta_{D_2O}} \sqrt{\frac{k_B T}{\kappa}} q^3 + \frac{(\tau {q_0}^3)^{-1}}{1 + (q - q_0)^2 \xi^{-2}} q^3 \qquad (S7)$$

in which the first term describes the contributions from the bending fluctuations discussed above and the second term is an empirical description for the contributions from the thickness fluctuations. The thickness fluctuations were modeled as a Lorentzian peak in which $\tau$ is related to the relaxation time of the thickness fluctuations, $q_0$ is the peak position, and $\xi$ is the half-width at half-maximum of the peak and is related to the fluctuation amplitude. Here we present the fractional amplitude, $\sigma_d$, as $\sigma_d = 2(\xi q_0)^{-1}$, or the full width half max of the peak in dynamics normalized by the peak position. (27, 28) Also, we note that the fitting did not account for the NSE instrument resolution and therefore the $K_A$ values calculated from $\sigma_d$ will be off by a proportionality constant. (22)

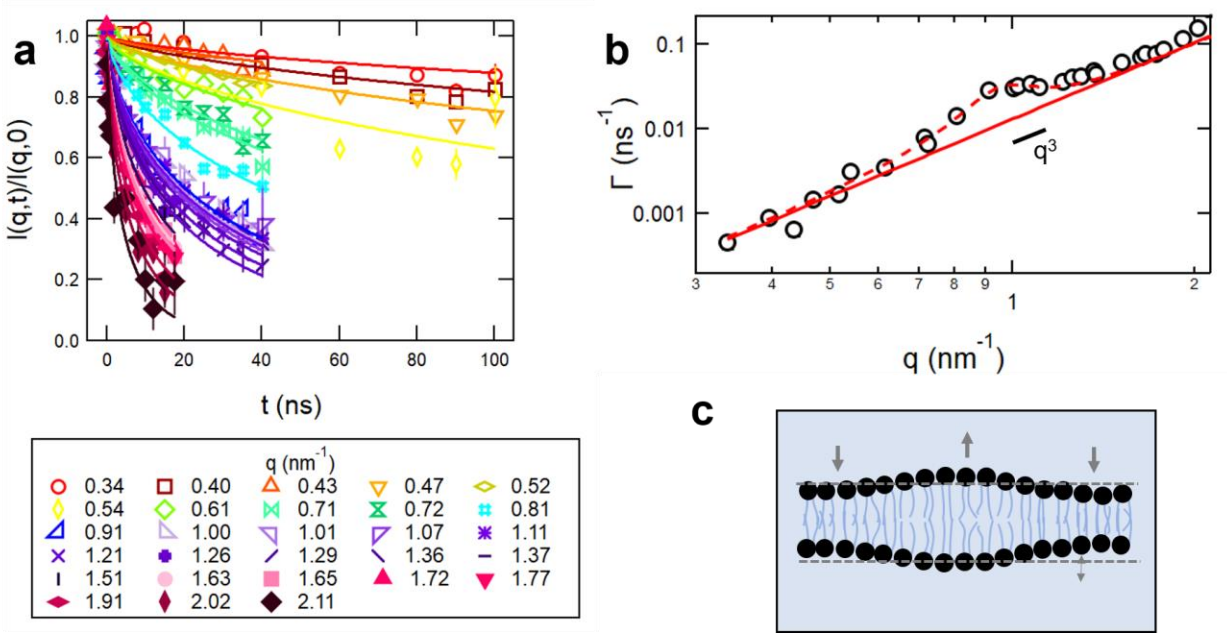


**Figure S5**. Neutron spin echo data (NSE) for thickness fluctuations measurements for $x_{DSPC}$ = 0.6 at $T$ = 65 °C ($T$ - $T_m$ = 20 °C). (**a**) Measured intermediate scattering function (points) and fits to a stretched exponential (lines) as well as the corresponding relaxation rates versus q in (**b**). The dashed line in (**b**) is the fit with Eq.S7 and the solid line is the calculated scaling for only bending fluctuations. The peak at q ≈ 1 nm$^{-1}$ is attributed to the collective thickness fluctuations. (**c**) Cartoon illustration of the scattering length density contrast between the tail-matched lipid bilayer and $D_2O$ solvent used to measure collective thickness fluctuations

Only two parameters were fit during the analysis of the thickness fluctuation data, τ and ξ. The peak position, $q_0$, was determined from SANS measurements and the bending modulus was determined from measurements of protiated lipids in $D_2O$ at the same relative temperature ($T - T_m$), in which $T_m$ is the main transition temperature for the pure component bilayers and the temperature onset of gel-fluid coexistence in the mixed lipid bilayers.(29) Representative NSE data and fits to Eq. S7 are shown in Figures S5 and S6, and the corresponding fit parameters are summarized in Table S5.

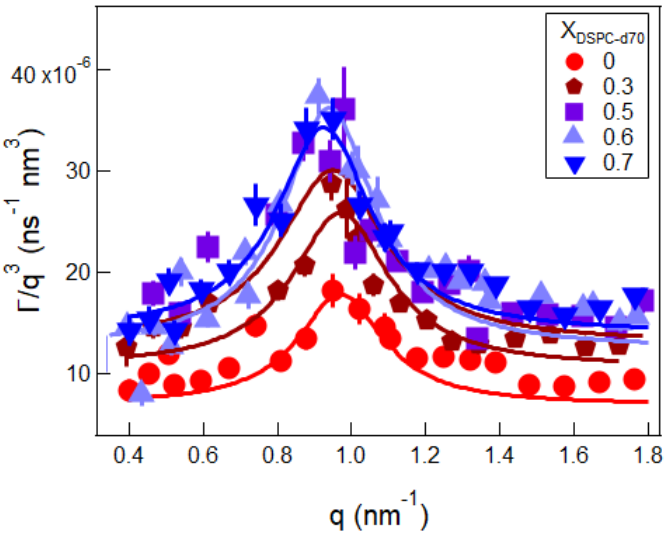


**Figure S6**. $q$-dependence of the NSE decay rate ($\Gamma$) normalized by $q^3$ for DMPC and the lipid mixtures at $T - T_m = 20$ °C. Solid lines represent the fits to the data according to Eq. S7. The peak in the plots at $q \approx 0.1$ Å$^{-1}$ is attributed to the membrane thickness fluctuations with a characteristic time scale determined by the peak height and a characteristic length scale determined by the peak width.

**Table S5.** Fit parameters for the NSE data in Figure S5 at $T - T_m = 20$ °C.

| $x_{DSPC-d70}$ | $\tau$ (ns) | $\sigma_d = 2(\xi q_0)^{-1}$ |
|---|---|---|
| 0 | 100.5 ± 12.3 | 0.26 ± 0.06 |
| 0.3 | 76.8 ± 5.5 | 0.32 ± 0.02 |
| 0.5 | 68.3 ± 5.1 | 0.36 ± 0.04 |
| 0.6 | 50.5 ± 2.8 | 0.32 ± 0.02 |
| 0.7 | 62.1 ± 4.8 | 0.34 ± 0.04 |

Importantly, the NSE data showed that the mixed lipid membranes are more dynamic than the constituent pure component membranes, independent of any model assumptions. Shown in Figure S7 are the characteristic parameters extracted from the NSE data on a linear-linear scale and the corresponding elastic and viscous properties plotted on log-log and log-linear scales, respectively. The solid lines are the best fits to the scaling relationships presented in the main text.

Figure S7a is the average $\left[(\Gamma/q^3)\cdot\eta_{D_2O}\right]^2$ which is proportional to $\tilde{\kappa}$ per Eq. S5. The $\eta_{D_2O}$ term accounts for the temperature dependence of the viscosity of $D_2O$ which dictates the dissipation through the solvent. The solid line is the predicted scaling for $\kappa \propto A_L^{-7}$ as discussed in the main text.

Figure S7b is the thickness fluctuation amplitude from the NSE data, $\sigma_d = 2(\xi q_0)^{-1}$, where $\xi$ is the Lorentzian peak width in Eq. S7. The fluctuation amplitude is greater for the mixtures than the pure component membranes (Table S5) and increase with increasing area per lipid, supporting that the membranes become more dynamic as they become less ordered. From the main text, $\sigma_d \propto K_A^{-1}$, and the solid line corresponds to $\sigma_d \propto A_L^3$.

Figure S7c is the thickness fluctuation relaxation time ($\tau$) in Eq. S7 determined from the height of the Lorentzian peak. The relaxation time is ≈ 20% to 40% faster in the mixtures compared to pure DMPC membranes (Table S5) and decreases with increasing $A_L$ (Figure S7c). As discussed in the text, $\tau \approx \eta_m/K_A$, and the solid line in Figure S6c is the best fit scaling to Eq. 2 in the text with $A_0 = 0.48$ nm$^2$ which was also used to predict the scaling for $\eta_m$.

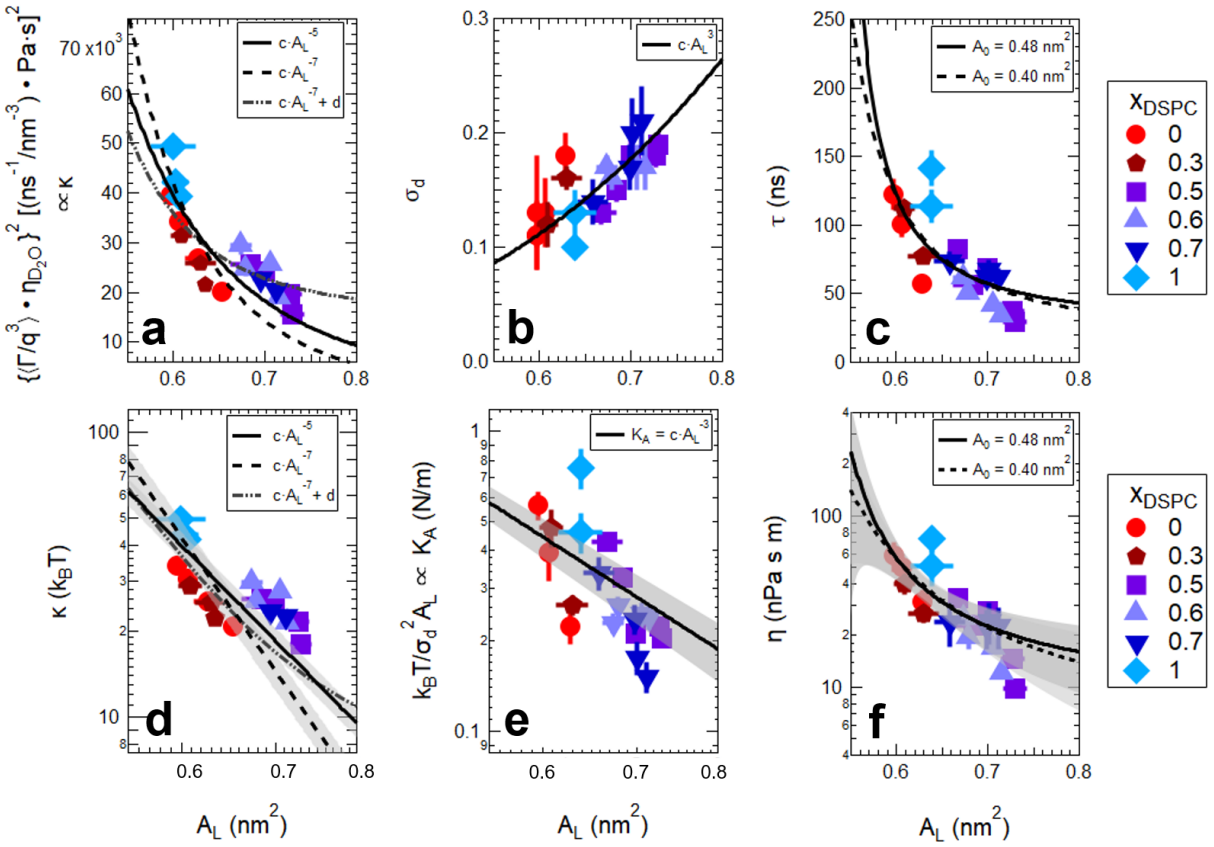


**Figure S7.** (top) Variables extracted from the NSE data for bending (**a**) and thickness (**b** and **c**) fluctuations plotted on linear-linear scales as a function of area per lipid and (bottom) corresponding membrane elastic and viscous properties. (**a**) Average decay rate normalized by $q^3$ determined from fits to the intermediate scattering function. (**b**) Thickness fluctuation amplitude and (**c**) relaxation time extracted from the peak width and height of the Lorentzian in Eq. S7, respectively. The corresponding elastic properties in panels (**d**) and (**e**) are plotted on log-log scales and the membrane viscosity data in (**f**) are plotted as log-linear scale. The points are the measured values for the different membrane compositions and temperatures while the solid lines are the scaling relationships from the corresponding elastic and viscous properties indicated in the legend and discussed in the main text. The shaded areas are the 95% confidence intervals. All points were weighted equally while fitting the scaling relationship.

## *References*


1. Greenwood AI, Tristram-Nagle S, & Nagle JF (2006) Partial molecular volumes of lipids and cholesterol. *Chem. Phys. Lipids* 143(1–2):1-10.
2. Heftberger P, Kollmitzer B, Rieder Alexander A, Amenitsch H, & Pabst G (2015) In Situ Determination of Structure and Fluctuations of Coexisting Fluid Membrane Domains. *Biophys. J.* 108(4):854-862.
3. Koenig BW & Gawrisch K (2005) Specific volumes of unsaturated phosphatidylcholines in the liquid crystalline lamellar phase. *Biochim. Biophys. Acta, Biomembr.* 1715(1):65-70.
4. Heimburg T (1998) Mechanical aspects of membrane thermodynamics. Estimation of the mechanical properties of lipid membranes close to the chain melting transition from calorimetry. *Biochim. Biophys. Acta, Biomembr.* 1415(1):147-162.
5. Ebel H, Grabitz P, & Heimburg T (2001) Enthalpy and Volume Changes in Lipid Membranes. I. The Proportionality of Heat and Volume Changes in the Lipid Melting Transition and Its Implication for the Elastic Constants‡. *J. Phys. Chem. B* 105(30):7353-7360.
6. Nagle JF (2013) Introductory Lecture: Basic quantities in model biomembranes. *Faraday discussions* 161:11-150.
7. Nagle JF & Tristram-Nagle S (2000) Structure of lipid bilayers. *Biochim. Biophys. Acta, Rev. Biomembr.* 1469(3):159-195.
8. Kučerka N, Nieh M-P, & Katsaras J (2011) Fluid phase lipid areas and bilayer thicknesses of commonly used phosphatidylcholines as a function of temperature. *Biochim. Biophys. Acta, Biomembr.* 1808(11):2761-2771.
9. Kučerka N, *et al.* (2008) Lipid Bilayer Structure Determined by the Simultaneous Analysis of Neutron and X-Ray Scattering Data. *Biophys. J.* 95(5):2356-2367.
10. Doktorova M, *et al.* (2019) Gramicidin Increases Lipid Flip-Flop in Symmetric and Asymmetric Lipid Vesicles. *Biophys. J.* 116(5):860-873.
11. Scott HL, *et al.* (2019) On the Mechanism of Bilayer Separation by Extrusion, or Why Your LUVs Are Not Really Unilamellar. *Biophys. J.* 117(8):1381-1386.
12. SasView ( *http://www.sasview.org/*).
13. Nagle JF, *et al.* (2019) Revisiting Volumes of Lipid Components in Bilayers. *J. Phys. Chem. B* 123(12):2697-2709.
14. Brzustowicz MR & Brunger AT (2005) X-ray scattering from unilamellar lipid vesicles. *Journal of Applied Crystallography* 38(1):126-131.
15. Krueger S, *et al.* (1995) Extending the Angular Range of Neutron Reflectivity Measurements from Planar Lipid Bilayers: Application to a Model Biological Membrane. *Langmuir* 11(8):3218-3222.
16. Kucerka N, Nagle JF, Feller SE, & Balgavy P (2004) Models to analyze small-angle neutron scattering from unilamellar lipid vesicles. *Phys. Rev. E* 69(5):9.
17. Pencer J, Krueger S, Adams CP, & Katsaras J (2006) Method of separated form factors for polydisperse vesicles. *Journal of Applied Crystallography* 39(3):293-303.
18. Kučerka N, *et al.* (Structure of Fully Hydrated Fluid Phase DMPC and DLPC Lipid Bilayers Using X-Ray Scattering from Oriented Multilamellar Arrays and from Unilamellar Vesicles. *Biophys. J.* 88(4):2626-2637.
19. Kučerka N, Heberle F, Pan J, & Katsaras J (2015) Structural Significance of Lipid Diversity as Studied by Small Angle Neutron and X-ray Scattering. *Membranes* 5(3):454.
20. Zilman AG & Granek R (1996) Undulations and dynamic structure factor of membranes. *Phys. Rev. Lett.* 77(23):4788-4791.
21. Watson MC & Brown Frank LH (2010) Interpreting Membrane Scattering Experiments at the Mesoscale: The Contribution of Dissipation within the Bilayer. *Biophys. J.* 98(6):L9-L11.

22. Nagao M, Kelley EG, Ashkar R, Bradbury R, & Butler PD (2017) Probing Elastic and Viscous Properties of Phospholipid Bilayers Using Neutron Spin Echo Spectroscopy. *The Journal of Physical Chemistry Letters* 8(19):4679-4684.
23. Nagao M (2009) Observation of local thickness fluctuations in surfactant membranes using neutron spin echo. *Phys. Rev. E* 80(3):031606.
24. Nagao M (2011) Temperature and scattering contrast dependencies of thickness fluctuations in surfactant membranes. *J. Chem. Phys.* 135(7):074704.
25. Woodka AC, Butler PD, Porcar L, Farago B, & Nagao M (2012) Lipid Bilayers and Membrane Dynamics: Insight into Thickness Fluctuations. *Phys. Rev. Lett.* 109(5):058102.
26. Ashkar R, *et al.* (2015) Tuning Membrane Thickness Fluctuations in Model Lipid Bilayers. *Biophys. J.* 109(1):106-112.
27. Carrillo J-MY, Katsaras J, Sumpter BG, & Ashkar R (2017) A Computational Approach for Modeling Neutron Scattering Data from Lipid Bilayers. *Journal of Chemical Theory and Computation* 13(2):916-925.
28. Lee V & Hawa T (2013) Investigation of the effect of bilayer membrane structures and fluctuation amplitudes on SANS/SAXS profile for short membrane wavelength. *J. Chem. Phys.* 139(12):124905.
29. Nagle JF, *et al.* (1998) Multiple mechanisms for critical behavior in the biologically relevant phase of lecithin bilayers. *Phys. Rev. E* 58(6):7769-7776.